


ORIGINAL WORK

Multi-omics Study of Hypoxic-Ischemic Brain Injury After Cardiopulmonary Resuscitation in Swine



Shuhang Yu^{1†}, Jiefeng Xu^{2†}, Chenghao Wu², Ying Zhu¹, Mengyuan Diao^{1*} and Wei Hu^{1*} 

© 2024 Springer Science+Business Media, LLC, part of Springer Nature and Neurocritical Care Society

Abstract

Background: Hypoxic-ischemic brain injury is a common cause of mortality after cardiac arrest (CA) and cardiopulmonary resuscitation; however, the specific underlying mechanisms are unclear. This study aimed to explore postresuscitation changes based on multi-omics profiling.

Methods: A CA swine model was established, and the neurological function was assessed at 24 h after resuscitation, followed by euthanizing animals. Their fecal, blood, and hippocampus samples were collected to analyze gut microbiota, metabolomics, and transcriptomics.

Results: The 16S ribosomal DNA sequencing showed that the microbiota composition and diversity changed after resuscitation, in which the abundance of *Akkermansia* and *Muribaculaceae_unclassified* increased while the abundance of *Bifidobacterium* and *Romboutsia* decreased. A relationship was observed between CA-related microbes and metabolites via integrated analysis of gut microbiota and metabolomics, in which *Escherichia-Shigella* was positively correlated with glycine. Combined metabolomics and transcriptomics analysis showed that glycine was positively correlated with genes involved in apoptosis, interleukin-17, mitogen-activated protein kinases, nuclear factor kappa B, and Toll-like receptor signal pathways.

Conclusions: Our results provided novel insight into the mechanism of hypoxic-ischemic brain injury after resuscitation, which is envisaged to help identify potential diagnostic and therapeutic markers.

Keywords: Cardiac arrest, Cardiopulmonary resuscitation, Gut microbiota, Metabolomics, Transcriptomics

Introduction

Cardiac arrest (CA) is a global health burden with high incidence and poor prognosis, with an annual in-hospital CA incidence of 292,000 [1] and 420,000 out of hospital CA (OHCA) in the United States [2]. Hypoxic-ischemic brain injury (HIBI) after resuscitation remains the primary cause of low survival [3]. Moreover, many CA

survivors have severe permanent neurological disability [4]. Understanding specific pathogenesis mechanisms involved in HIBI is limited, drastically hindering the development of novel treatment strategies. Therefore, in-depth research about pathophysiologic mechanisms and novel therapeutic target of HIBI is required.

The current mainstream view is that HIBI pathophysiology is a “two-hit” model [5]. The primary injury results from the immediate cessation of oxygen delivery. Although the weight of the brain only accounts for 2% of the whole body, the brain consumes 20% of cardiac output to maintain function [6]. Glucose is an essential nutrient for brain function maintenance, and glucose transport depends on cerebral blood flow because the

*Correspondence: diaomengyuan@hospital.westlake.edu.cn; huwei@hospital.westlake.edu.cn

[†]Shuhang Yu and Jiefeng Xu have contributed equally to this work.

¹ Department of Critical Care Medicine, Hangzhou First People's Hospital, Zhejiang University School of Medicine, Hangzhou, China

Full list of author information is available at the end of the article

brain does not store glucose [7]. When CA occurs, the cessation of cerebral blood flow will lead to an immediate interruption of brain activity, neurogenic hypoglycemia, and metabolic disorders within a few minutes, resulting in cell death [8]. Previous studies have shown that classical mechanisms, such as energy metabolism disorder, calcium overload, oxidative stress, and excitotoxicity, play an important role in HIBI [9]. Secondary injury results from an imbalance in oxygen delivery and use after resuscitation, taking place in the hours and days following the initial CA and reperfusion, ultimately causing neuronal death. A number of factors may be contributing to this secondary injury, including reperfusion injury, microcirculation dysfunction, impaired cerebral autoregulation, hypoxemia, hyperoxia, hyperthermia, and concomitant anemia [5].

Recently, interest has been drawn toward the role of the gut microbiota as a potential novel contributor to HIBI. Accumulating evidences suggested the pathogenesis of central nervous system (CNS) diseases being associated with intestinal microbiota, such as depression [10], stroke [11], and sepsis-associated encephalopathy [12]. Moreover, the latest published reports suggested regulation of CNS by intestinal microbiota via several aspects, including direct regulation of the enteric nervous system, metabolites produced by microbiota entering the CNS through the blood–brain barrier, and microbial-associated molecular patterns or metabolites modulating the immune system [13]. Similarly, it was reported that the gut microbiota of old mice worsened ischemic brain injury and inflammation via increased valeric acid and interleukin-17 (IL-17) in the blood [14]. Several specific microbiotas, such as *Peptococcaceae* and *Prevotellaceae*, were also found to be related to neurological deficits in ischemic stroke [15]. However, studies on the role of gut microbiota in HIBI after resuscitation pathogenesis are limited and need further investigation.

Metabolomics profiling revealed brain metabolome dysfunction onset predominantly after resuscitation [16]. A study showed changes in the tricarboxylic acid cycle, tryptophan and kynurenic acid, bile acid, acylcarnitine, fatty acid, and phospholipid metabolites after resuscitation [17]; moreover, tricarboxylic acid cycle metabolites could describe the variance between patients with good and poor outcome [18]. As described earlier, gut microbiota-produced metabolites play an important role in CNS diseases. For example, the major tryptophan metabolism pathways, including the kynurenine pathway, are under the direct or indirect control of the microbiota [19], whereas the degree of peripheral activation of the kynurenine pathway may predict postresuscitation neurological function [20]. In addition, gut microbiome-dependent and dietary-associated metabolite,

namely trimethylamine-N-oxide (TMAO), was related to in-hospital mortality of patients with OHCA [21]. An increasing number of studies focused on the relationship between the gut microbiota and metabolites; however, the interaction between the gut microbiota and metabolites in CA is still unclear.

Transcriptomic analysis is significant in understanding gene regulation, disease occurrence and development, drug research and development, and other fields. Differences in plasma transcriptomic response between favorable and unfavorable neurological outcomes in patients with CA were observed in clinical trials [22]. Similarly, another study identified three plasma biomarkers, mitogen-activated protein kinase (MAPK)-3, B-cell lymphoma-2, and serine/threonine protein kinase B-1, associated with poor neurological postresuscitation outcomes [23]. Transcriptome sequencing also showed changed mitochondrial function in H2C9 cells after hypoxia [24]. Thus, deep insight into the transcriptome is crucial in CA and resuscitation.

Therefore, to clarify the expression characteristics of gut microbiota and metabolites after resuscitation, as well as the changes of brain gene expression, is of great significance for exploring the mechanism of HIBI. The current study established a ventricular fibrillation (VF)-induced CA swine model to investigate the relationship between gut microbiota, plasma metabolites, and hippocampal gene expression. The results of this study are envisaged to help characterize altered microbiota patterns, metabolites, and hippocampal transcriptome after resuscitation, potentially providing future insight into CA therapeutic targets.

Methods

Animals

Briefly, 12 six-month-old male white domestic swine (weighing 39.3 ± 2.1 kg) were obtained from Shanghai Jiagan Biotechnology Inc. (Shanghai, China) and randomly divided into two groups: sham ($n=6$) and CA ($n=6$). All animals were kept on fasting overnight with free access to water before experimentation. All animals underwent general preparation, including anesthesia, endotracheal intubation, and femoral arteriovenous catheterization. The sham animals were not subjected to CA and CPR procedures, while the CA group received 10 min of CA followed by 6 min of CPR. The experimental flow chart was showed in Supplementary Fig. 1. The experimental protocol and procedures were approved by the Institutional Animal Care and Use Committee of the Second Affiliated Hospital, Zhejiang University School of Medicine. The experiment followed the Guide for the Care and Use of Laboratory Animals prepared by the Institute of Laboratory Animal Resources, published by the National

Institutes of Health. The work was reported according to Animal Research: Reporting of In Vivo Experiments guideline.

Anesthesia and Surgeries

After initial intramuscular midazolam (0.4–0.5 mg/kg) followed by intravenous (I/V) propofol (2 mg/kg), endotracheal tubes (7.0 mm) were inserted into the trachea. Anesthesia was maintained by continuous I/V propofol (4 mg/kg) via an I/V pump. After the animals were intubated, mechanical ventilation was initiated with volume-controlled ventilation (Oxylog 3000 plus, Dräger, Luebeck, Germany). The ventilator parameters were as follows: the tidal volume was 12 mL/kg, the peak flow was 40 L/min, and a fraction of inspired oxygen (FiO₂) was 0.21. Lead II electrocardiogram was continuously recorded. To measure cardiac function at the indicated time points, a 7F central venous catheter (Abbott Critical Care # 41216, Chicago, IL) was placed in the left external jugular vein, and another 4F thermistor-tipped arterial catheter (Abbott Critical Care # 41216, Chicago, IL) was placed into the left femoral artery. Both catheters were connected to the Pulse index Continuous Cardiac Output Monitor system (BeneVision N22, Mindray, Shenzhen, China) to record stroke volume (SV) and global ejection function (GEF). To measure mean arterial pressure (MAP), an 8F catheter (6523, C.R. Bard Inc., Salt Lake, UT) was inserted into the thoracic aorta through the right femoral artery. The VF was induced via a 5F pacing catheter (EP Technologies Inc., Mountain View, CA) placed into the right ventricle through the right external jugular vein. The positions of all the catheters were confirmed by characteristic pressure morphology. All the catheters were filled with heparin saline (5 IU/mL) and intermittently flushed. A thermal probe was inserted into the rectum to record temperature, and the rectum temperature was maintained at 38.0 ± 0.5 °C in all the animals. The hemodynamic parameters at baseline (heart rate [HR], mean arterial pressure [MAP], SV, and GEF) was recorded.

VF-Induced CA

The VF-induced CA swine model development is described in our previous study [25]. Briefly, 10 min before VF induction, baseline measurements were recorded, and VF was induced by a 1 mA alternating current delivered to the right ventricular endocardium. Successful CA was indicated by When VF on ECG and MAP ≤ 20 mmHg. Mechanical ventilation was discontinued after VF induction. The pace catheter was removed before CPR. Following 10 min of untreated VF, manual chest compression was initiated, accompanied by ventilation at a 30:2 ratio, performed by a bag respirator

attached to the endotracheal tube. The depth and rate of chest compression were monitored by an E Series Monitor Defibrillator (PlamCPR, Sunlife, Suzhou, China) to guarantee a depth of 50–60 mm and a rate of 100–120/min. After 2 min of CPR, epinephrine (20 µg/kg) was injected as a bolus, and after 6 min of CPR, a single 150-J electrical shock was achieved for defibrillation using E Series Monitor Defibrillator. Return of spontaneous circulation (ROSC) was defined as the appearance of an organized rhythm with MAP > 50 mmHg that persisted for more than 5 min. If ROSC was not observed, CPR and ventilation were continued for an additional 2 min before the next defibrillation and were repeated until the occurrence of CPR for up to 10 min. Repeating doses of epinephrine were administered at 4 min intervals after the first injection. Following ROSC, hemodynamic parameters (HR, MAP, SV and GEF) was recorded at 1, 2, 4 h after resuscitation. All catheters were removed at 4 h after resuscitation, and animals were transferred to closed cages for 20 h of observation.

Neurological Deficit Scores

Two trained investigators evaluated the neurological function of the animals blinded to the study protocol 24 h after resuscitation as previously described [26]. The parameters considered for neurological activity, including consciousness, respiration, motor response, muscle tone, standing, walking, and restraint, were evaluated (Supplementary Table 1). The scores range from 0 (normal) to 400 (brain death).

Sample Collecting

All animals were euthanized at 24 h after resuscitation with an I/V propofol (3 mg/kg) followed by 10 mL of potassium chloride (10 mol/L). The blood, hippocampus, and fecal specimens were harvested and stored in liquid nitrogen. All blood and tissue samples were analyzed by experienced technicians blinded to the study.

Intestinal Microbiota Analysis

DNA Extractions

DNA from different fecal samples was extracted using the E.Z.N.A. Stool DNA Kit (D4015, Omega, Inc., USA) according to the manufacturer's instructions, while nuclear-free water was used as a blank. The reagent, designed to uncover DNA from trace amounts of sample, has been shown to be effective for the preparation of DNA of most bacteria. The total DNA was eluted in 50 µL of elution buffer and stored at – 80 °C until PCR analysis (LC-Bio Technology Co., Ltd, Hang Zhou, Zhejiang Province, China).

PCR Amplification and 16S rDNA Sequencing

The V3–V4 region of the 16S rRNA was amplified using 341F (5'-CCTACGGGNGGCWGCAG-3') and 805R primers (5'-GACTACHVGGGTATCTAATCC-3'). PCR amplification was performed in a total volume of 25 μ L reaction mixture containing 25 ng of template DNA, 12.5 μ L PCR premix, 2.5 μ L of each primer, and PCR-grade water to adjust the volume. The PCR conditions to amplify the prokaryotic 16S fragments consisted of an initial denaturation at 98 °C for 30 s; 32 cycles of denaturation at 98 °C for 10 s, annealing at 54 °C for 30 s, and extension at 72 °C for 45 s, followed by final extension at 72 °C for 10 min. The PCR products were confirmed with 2% agarose gel electrophoresis. Throughout the DNA extraction process, ultrapure water instead of a sample solution was used as a negative control to exclude the possibility of false positive results. The PCR products were purified by AMPure XT beads (Beckman Coulter Genomics, Danvers, MA, USA) and quantified by Qubit (Invitrogen, USA). The amplicon pools were prepared for sequencing, and the size and quantity of the amplicon library were assessed on Agilent 2100 Bioanalyzer (Agilent, USA) and with the Library Quantification Kit for Illumina (Kapa Biosciences, Woburn, MA, USA), respectively. The libraries were sequenced on the NovaSeq PE250 platform.

Bioinformatics and Statistical Analysis

Samples were sequenced on an Illumina NovaSeq platform according to the manufacturer's instructions (LC-Bio). Paired-end reads were assigned to samples based on their unique barcode and truncated by cutting off the barcode and primer sequence and were merged using FLASH. Quality filtering on the raw reads was performed under specific filtering conditions to obtain high-quality clean tags according to the fqtrim (v0.94). Chimeric sequences were filtered using Vsearch software (v2.3.4). Feature table and sequence were obtained following dereplication using DADA2. Alpha and beta diversity were calculated by randomly normalizing them to identical sequences. Then, according to the SILVA (release 132) classifier, feature abundance was normalized using the relative abundance of each sample. Alpha diversity was applied in analyzing the complexity of species diversity for a sample through five indices, including Chao1, Observed species, Goods coverage, Shannon, and Simpson, while alpha and beta diversities were calculated with QIIME2, and graphs were drawn using the R package. Blast was used for sequence alignment, and the feature sequences were annotated with the SILVA database for each representative sequence. Other diagrams were generated using the R package (v3.5.2).

Metabolomics Analysis

Extraction of Metabolites

The collected plasma samples were removed, thawed on ice, and metabolites were extracted using 50% methanol buffer. Briefly, 100 μ L of the sample was mixed with 4000 μ L of precooled 50% methanol in a 1.5 mL EP tube, vortexed for 1 min, and incubated at -20 °C for 30 min. The extraction mixture was then centrifuged at 20,000g for 10 min, and 400 μ L supernatants were transferred into new EP tubes, freeze-dried (2 h), and then stored at -80 °C before the LC–MS/MS analysis. In addition, after being dissolved in 100 μ L 80% iced methanol, pooled QC samples were prepared by mixing 10 μ L of each extraction mixture.

First group samples to ensure that different groups are cross-sorted on the machine; all samples were analyzed on LC–MS/MS system following machine orders. All chromatographic separations were performed using a Thermo Scientific UltiMate 3000 HPLC. An ACQUITY UPLC T3 column (100 mm \times 2.1 mm, 1.8 μ m, Waters, UK) was used for reversed-phase separation. The column oven was maintained at 50 °C. The mobile phase comprised water and 0.1% formic acid as phase A, while acetonitrile and 0.1% formic acid as phase B at a flow rate of 0.3 mL/min. Elution was conducted under gradient elution conditions set as follows: 2% B for 0–0.8 min; 2–70% B for 0.8–2.8 min; 70–90% B for 2.8–5.6 min; 90–100% B for 5.6–8 min; 100–2% B for 8–8.1 min; and 2% B for 8.1–10 min. The injection volume for each sample was 4 μ L. Initially, one or two WASH samples were scanned, followed by 3–4 QCs, then QC was inserted for every 10 samples scanned, and finally, 2 QCs were inserted.

A high-resolution tandem mass spectrometer (Q-Exactive, Thermo Scientific) was used to collect the metabolites eluted from the column's first- and secondary-order spectrum data. The Q-Exactive was operated in both positive and negative ion modes. Precursor spectra (70–1050 m/z) were collected at 70,000 resolutions to hit an automatic gain control (AGC) target of 3e6. The maximum injection time was set to 100 ms. A top 3 configuration to acquire data was set in data dependent acquisition mode. Fragment spectra were collected at 17,500 resolution to hit an AGC target of 1e5 with a maximum inject time of 50 ms. Fragmentation energy (stepped nce) was set as 20, 40, and 60 eV, whereas electrospray ion source parameter settings were as follows: spray voltage (|KV|) was 4000 (positive ion mode) and 4000 (negative ion mode); the sheath gas flow rate was 35; the aux gas flow rate was 10; the capillary temperature was 320 °C.

Metabolomics Data Processing and Analysis

The acquired mass spectrum raw data (.raw files) was imported into Compound Discoverer 3.1.0 (Thermo

Fisher Scientific, USA) for data pretreatments, including peak extraction, retention time correction within and between groups, adduct ion merging, fill gaps, background peak labeling, and metabolite identification. Each ion was identified by combining retention time and m/z data. Intensities of each peak were recorded, and information such as feature molecular weight, retention time, peak area, and identification results were exported. The online Kyoto Encyclopedia of Genes and Genomes (KEGG) and Human Metabolome Database (HMDB) databases annotated the metabolites by matching the exact molecular mass data, name, and formula of samples with those from the database. The metabolite was annotated if the mass difference between the observed and database values was less than 10 ppm.

The intensity of peak data was further preprocessed by metaX software. Those features detected in less than 50% of QC samples or 80% of biological samples were removed, and the remaining peaks with missing values were credited with the k -nearest neighbor algorithm to improve the data quality further. Principal component analysis (PCA) was performed for outlier detection and batch effects evaluation using the preprocessed data sets. Probabilistic Quotient Normalization was used to normalize the data to obtain the normalized ion intensity data of each sample. Quality control-based robust LOESS signal correction was fitted to the QC data concerning the order of injection to minimize signal intensity drift over time. In addition, the coefficient of variation of the metabolic features was calculated across all QC samples, and those >30% were removed.

Student's t -tests were conducted to detect differences in metabolite concentrations between two phenotypes. The P value was adjusted for multiple tests using a false discovery rate (FDR) (Benjamini-Hochberg). Supervised PLS-DA was conducted through metaX to discriminate the different variables between groups, and the variable important in projection (VIP) value was calculated. A VIP cut-off value of 1.0 was used to select important features. KEGG enrichment analysis was performed on significantly different metabolites (satisfying ratio ≥ 2 or ratio $\leq 1/2$ and P value ≤ 0.05 and VIP > 1). Spearman rank correlation analysis was performed to detect the correlations between microbiota and metabolites using R package (v3.6.3).

Transcriptome Analysis

RNA Extraction Library Construction and Sequencing

Total RNA was extracted using Trizol reagent (thermofisher, 15596018) following the manufacturer's instructions. The total RNA quantity and purity were analyzed by Bioanalyzer 2100 and RNA 6000 Nano LabChip Kit (Agilent, CA, USA, 5067-1511), and

high-quality RNA samples with RIN number >7.0 were used to construct the sequencing library. After total RNA extraction, mRNA was purified from total RNA (5 μ g) using Dynabeads Oligo (dT) (Thermo Fisher, CA, USA) with two rounds of purification. Following purification, the mRNA was fragmented into short fragments using divalent cations under elevated temperature (Magnesium RNA Fragmentation Module (NEB, cat. e6150, USA) under 94 °C 5–7 min). The cleaved RNA fragments were then reverse-transcribed to create the cDNA by SuperScript™ II Reverse Transcriptase (Invitrogen, cat.1896649, USA), which were next used to synthesize U-labeled second-stranded DNAs with *E. coli* DNA polymerase I (NEB, cat.m0209, USA), RNase H (NEB, cat. m0297, USA), and dUTP solution (Thermo Fisher, cat. R0133, USA). An A-base was then added to the blunt ends of each strand, preparing them for ligation to the indexed adapters. Each adapter contained a T-base overhang for ligating the adapter to the A-tailed fragmented DNA. Dual-index adapters were ligated to the fragments, and size selection was performed with AMPureXP beads. After the heat-labile UDG enzyme (NEB, cat.m0280, USA) treatment of the U-labeled second-stranded DNAs, the ligated products were amplified with PCR using following conditions: initial denaturation at 95 °C for 3 min; 8 cycles of denaturation at 98 °C for 15 s, annealing at 60 °C for 15 s; extension at 72 °C for 30 s; and then final extension at 72 °C for 5 min. The average insert size for the final cDNA libraries was 300 ± 50 bp. Finally, we performed the 2×150 bp paired-end sequencing (PE150) on an Illumina Novaseq™ 6000 (LC-Bio Technology CO., Ltd., Hangzhou, China) per the vendor's recommended protocol.

Bioinformatics and Statistical Analysis

Reads obtained from the sequencing machines included raw reads containing adapters or low-quality bases, which will affect the following assembly and analysis. Thus, to get a high-quality clean read, reads were further filtered by Cutadapt (<https://cutadapt.readthedocs.io/en/stable/>, version: cutadapt-1.9). The parameters were as follows: (1) removing reads containing adapters; (2) removing reads containing polyA and polyG; (3) removing reads containing more than 5% of unknown nucleotides (N); (4) removing low-quality reads containing more than 20% of low-quality (Q value ≤ 20) bases. The sequence quality was verified using FastQC (<http://www.bioinformatics.babraham.ac.uk/projects/fastqc/>, version: 0.11.9). Including Q20, Q30, and GC-content of the clean data, resulting in producing cleaned total G bp and paired-end reads.

We aligned reads of all samples to the swine reference genome using HISAT2 (<https://daehwankimlab.github.io>).

io/hisat2, version: hisat2-2.0.4) package, which initially removed a portion of the reads based on quality information accompanying each read followed by mapping the reads to the reference genome. HISAT2 allowed multiple alignments per read (up to 20 by default) and a maximum of two mismatches when mapping the reads to the reference. HISAT2 built a database of potential splice junctions, which were confirmed by comparing the previously unmapped reads against the database of putative junctions.

The mapped reads of each sample were assembled using StringTie (<http://ccb.jhu.edu/software/stringtie>, version: stringtie-1.3.4d) with default parameters, followed by merging all sample transcriptomes for constructing a comprehensive transcriptome using gffcompare software (<http://ccb.jhu.edu/software/stringtie/gffcompare.shtml>, version: gffcompare-0.9.8). After the final transcriptome was generated, StringTie and ballgown (<http://www.bioconductor.org/packages/release/bioc/html/ballgown.html>) were used to estimate the expression levels of all transcripts, and expression abundance was performed for mRNAs by calculating FPKM (fragment per kilobase of transcript per million mapped reads) value. PCA was performed to reveal the relationship of the samples by the princomp function of R (<http://www.r-project.org/>).

Differentially expressed genes (DEGs) were analyzed using DESeq2 software between two groups. The genes with FDR parameters below 0.05 and absolute fold change ≥ 2 were considered DEGs. The DEGs were then subjected to GO enrichment (<http://www.geneontology.org/>) and KEGG (<https://www.kegg.jp/kegg/>) pathways analysis for exploring the biological functions and potential pathways of identified DEGs. The GO category and annotation list were determined using Fisher's exact test. The gene association network was constructed by the Search Tool for the Retrieval of Interacting Genes/Proteins (STRING database, <https://string-db.org/>, version 11.0).

Results

Physiologic, Hemodynamic, and Resuscitation Data

The baseline data are shown in Table 1. Results indicated no significant differences in body weight, heart rate, MAP, SV, and GEF between the two groups on baseline data (Table 1).

Figure 1 showed the hemodynamic changes during the first 4 h after resuscitation. Compared to sham group, the HR of CA group was significantly higher after resuscitation, while the SV and GEF were significantly lower. In addition, the MAP of CA group was significantly lower than that of sham group at 4 h after resuscitation. Intra-group comparisons of HR, MAP, SV and GEF revealed no significant differences at any time point in the sham

Table 1 Baseline data

	CA	Sham
Body weight (kg)	38.3 ± 2.4	40.2 ± 1.3
HR (bpm)	87.2 ± 5.1	80.0 ± 6.3
MAP (mmHg)	103.8 ± 4.1	99.5 ± 6.6
SV (ml)	41.8 ± 6.6	42.2 ± 1.9
GEF (%)	34.5 ± 5.1	38.3 ± 4.1

HR heart rate, MAP mean atrial pressure, SV stroke volume, GEF Global ejection fraction

group. Conversely, compared to baseline values, the HR in the CA group at 1 h after resuscitation was significantly higher, while the MAP at 4 h after resuscitation was significantly lower. Similarly, the SV and GEF at selected time points in CA group were significantly lower when compared to baseline values, and both reached the lowest value at 1 h after resuscitation.

Resuscitation data were also recorded. In CA group, the average CPR duration was 6.7 ± 1.0 min, epinephrine dosage was 1.8 ± 0.3 mg and defibrillation times were 1.3 ± 0.5 times respectively.

The neurological deficit score (NDS) results are shown in Fig. 2. The NDS significantly increased compared to the sham group (162.5 ± 49.1 vs. 15.8 ± 5.8 , $P < 0.05$), indicating pstresuscitation neurological injury.

Changes in the Gut Microbiome of CA Swine

The composition of the gut microbiome was detected by 16S rDNA gene sequencing. In general, 12 samples were analyzed, and 805,770 high-quality sequences were detected. The rarefaction curves tend to be flattened, indicating adequate sequencing depth. Alpha diversity indices, including Observed species, Chao1, Shannon, and Simpson, showed no significant difference between CA and sham group ($P > 0.05$, Table 2). However, the beta diversity was different between the two groups. The unweighted UniFrac PCoA analysis displayed the apparent separation between the two groups (Fig. 3A), while a significant difference was observed for *Firmicutes/Bacteroidetes* ratio (F/B ratio) between two groups (student's *t*-test, $P = 0.047$, Supplementary Fig. 2). These data suggested that CA treatment may alter gut microbiome richness and diversity in swine to some extent.

At the phylum level, *Firmicutes* and *Bacteroidetes* were two dominant phyla in both CA and sham groups (Supplementary Fig. 3A). The abundance of *Actinobacteria* and *Planctomycetes* was found to decrease while increasing for *Verrucomicrobia* (Supplementary Fig. 3B) compared to the sham group. At the genus level, *Muribaculaceae_unclassified* and *Lactobacillus* dominated in both groups. There was a total of 29 differentially

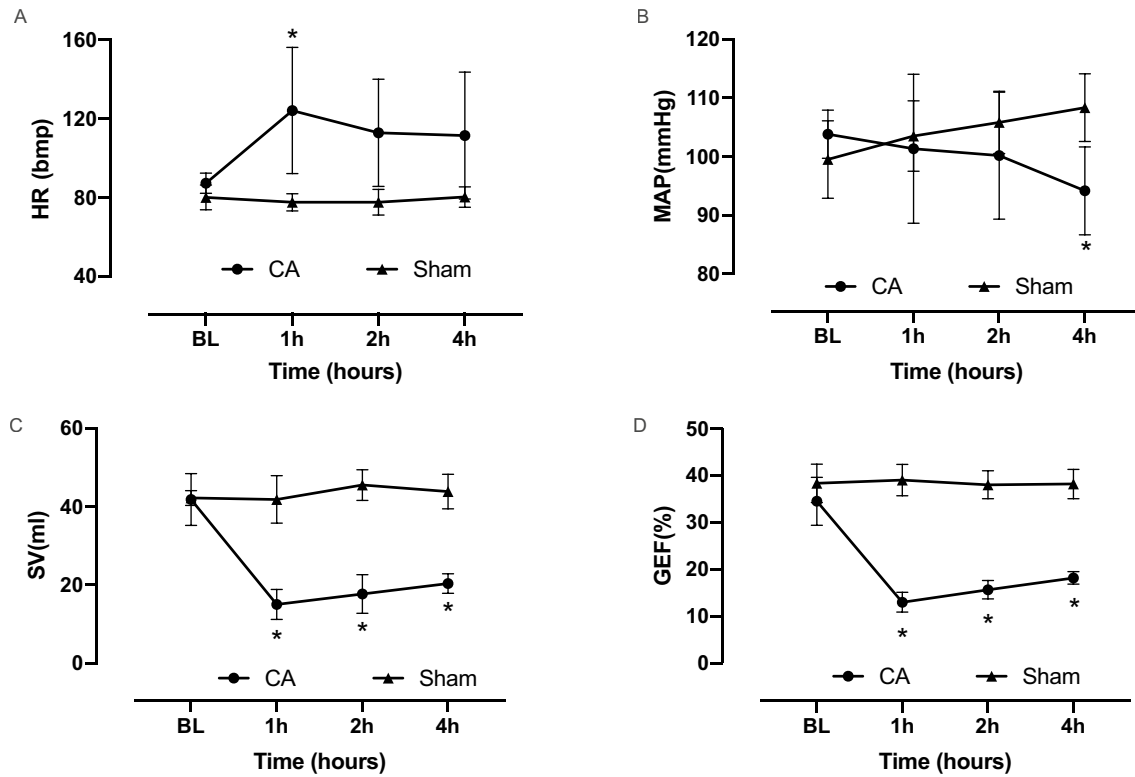


Fig. 1 Hemodynamics changes during the first 4 h after resuscitation between the two groups. **A** Heart rate, **B** mean atrial pressure, **C** stroke volume and **D** global ejection fraction. *A significant change from baseline in the CA group ($P < 0.05$). HR, heart rate; MAP, mean atrial pressure; SV, stroke volume; GEF, Global ejection fraction

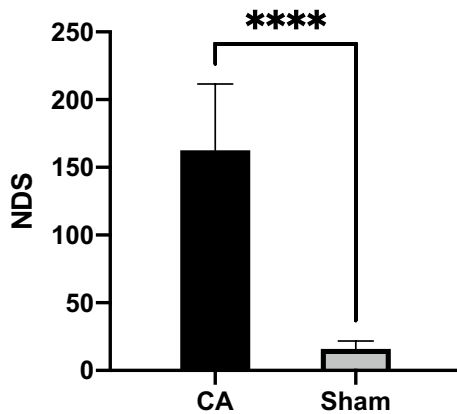


Fig. 2 Neurologic deficit scores at 24 h after resuscitation. **** $P < 0.0001$ versus Sham group. NDS, neurological deficit score

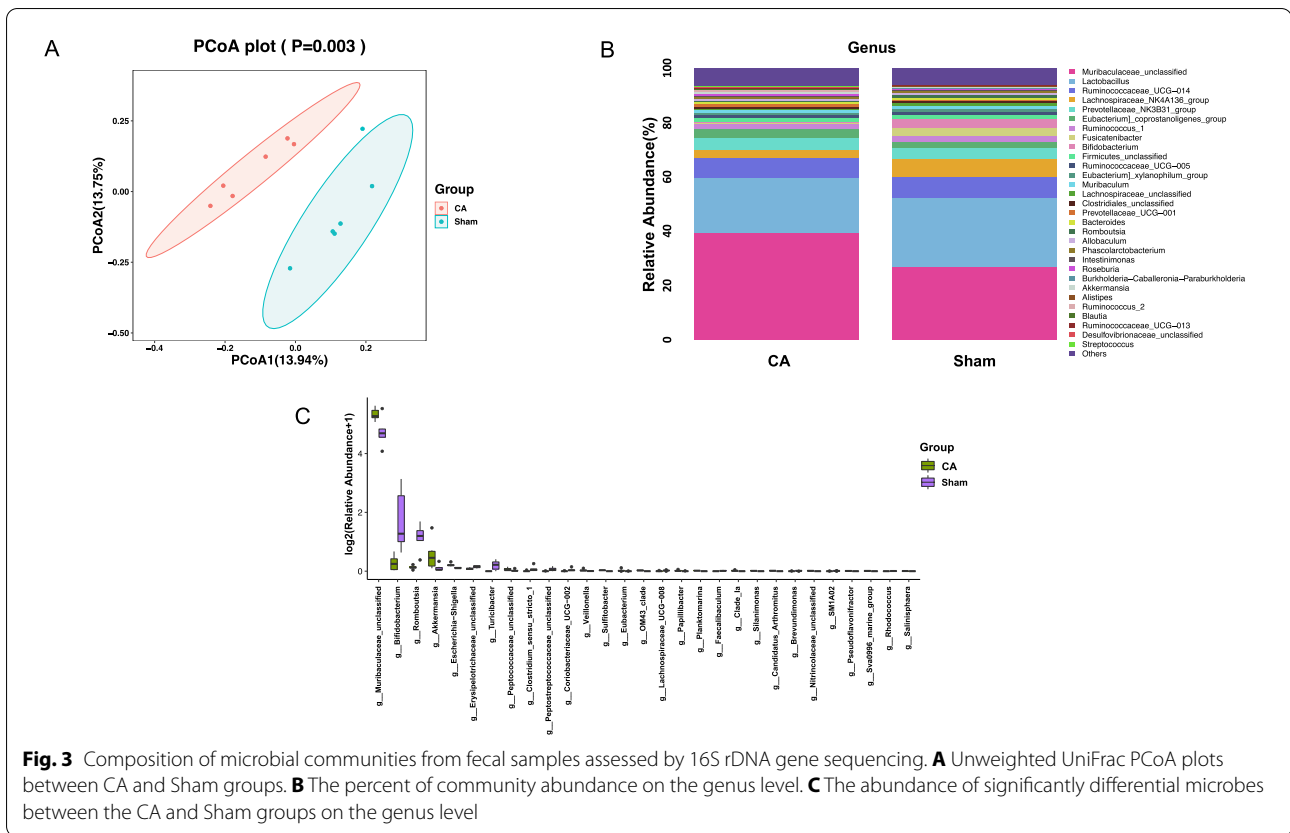
Table 2 Alpha diversity between CA and Sham group

Group	observed_otus	shannon	simpson	chao1	goods_coverage
CA	758.00	6.86	0.97	762.06	1.00
sham	673.50	6.68	0.97	675.46	1.00
P value	0.39	0.59	0.94	0.39	0.23

we found 19 marker bacterial taxa (Fig. 4A,B). Similarly, at the genus level, there were 4 potential biomarkers in the CA group: *Bifidobacterium*, *Romboutsia*, *Akkermansia*, and *Muribaculaceae_unclassified*. Moreover, *Akkermansia_muciniphila* (*A. muciniphila*) was found to increase in CA compared to the sham group.

The KEGG pathways associated with gut microbiota were predicted using PICRUSt2 to investigate any functional changes between CA and sham groups (Fig. 4C). Results indicated significant differences between the two groups in one second-level and 15 third-level classification KEGG pathways. In second-level, the enzyme families was significantly differed between the two groups.

abundant genera (Fig. 3B), among which the abundance of *Muribaculaceae_unclassified*, *Akkermansia* and *Escherichia-Shigella* were found to increase while *Bifidobacterium* and *Romboutsia* were decreased when compared to sham group (Fig. 3C). Using the LefSe method,



In third-level classification, indole alkaloid biosynthesis, bacterial invasion of epithelial cells, protein folding and associated processing, and pathogenic *Escherichia coli* infection were abundant in the CA group, while transcription-related proteins were abundant in the sham group.

Plasma Metabolite Profiles of CA Swine

Untargeted metabolomics analysis was performed using LC-MS/MS after plasma sample extraction. The PCA revealed two different clusters, indicating the different metabolic profiles of the CA and sham groups (Fig. 5A,B). Combined with the fold change (ratio ≥ 2 or ratio ≤ 0.5) and VIP (≥ 1), a total of 221 metabolites were considered as differential metabolites. The volcano plots visually displayed the differences in metabolic patterns, with 134 upregulated and 87 downregulated metabolites in the CA group, compared to the sham group (Fig. 5C).

Among the differential metabolites, 13 amino acids and derivatives were identified, of which glycine and 5-methoxyindoleacetate were upregulated, while indole, 3-indoleacetic acid and D-lombricine were downregulated. Similarly, a total of 24 lipid molecules were identified, among which 10 acylcarnitines

(short-chain acylcarnitine (C2:0, C4-OH), medium-chain acylcarnitine (C6:0, C6-OH, C10:0), and long-chain acylcarnitine (C16:0, C16:2, C16-OH, C18:0, C18:2)) and 4 fatty acids (tetradecanedioic acid, palmitoleic acid, hexadecanedioic acid, and suberic acid) were upregulated and 1 lysophosphatidylcholine (LPC) was downregulated.

Among the 221 identified metabolites, 59 were annotated in the KEGG compound database, and then KEGG pathway enrichment analysis was applied. The differential metabolites were enriched to 26 KEGG pathways, of which 4 pathways were significantly enriched, including porphyrin and chlorophyll metabolism, tryptophan metabolism, glycine, serine and threonine metabolism, and phenylalanine metabolism pathway (Fig. 5D). Metabolites in porphyrin and chlorophyll metabolism pathway were identified as glycine, bilirubin, biliverdin and (3z)-phytychromobilin. Metabolites in tryptophan metabolic pathway were identified as indole, 3-indoleacetic acid and 5-methoxyindoleacetate. Metabolites in glycine, serine and threonine pathway were identified as glycine and D-lombricine. Metabolites of phenylalanine metabolism pathway were identified as salicylic acid and hippuric acid.

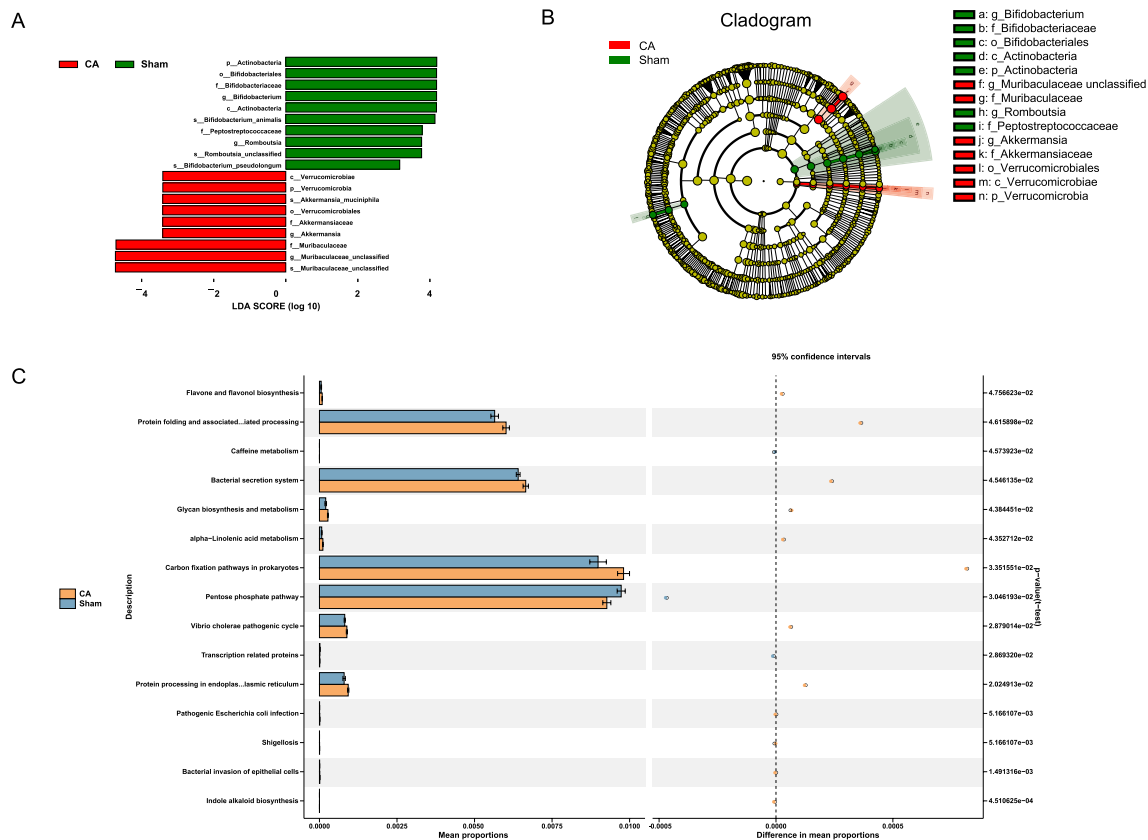


Fig. 4 The LEfSe analysis and PICRUSt2 of gut microbiota between CA and Sham groups. **A** LDA score distribution diagram. The LDA score greater than 2 indicates significantly different existing in species between two groups. The length of the histogram represents the size of the impact of significantly different species. **B** Cladogram of different species. The circle radiating from inside to outside represents the classification from the phylum to the genus level. Each small circle represents a classification at that level at different classification levels. The diameter of the small circle is proportional to the relative abundance. **C** Abundances of KEGG pathways in level-3 of the functional prediction by PICRUSt2

Correlations Between the Gut Microbiome and Metabolites

To evaluate the potential relationships between gut microbiota and KEGG annotated plasma metabolites, we performed spearman rank correlation analysis.

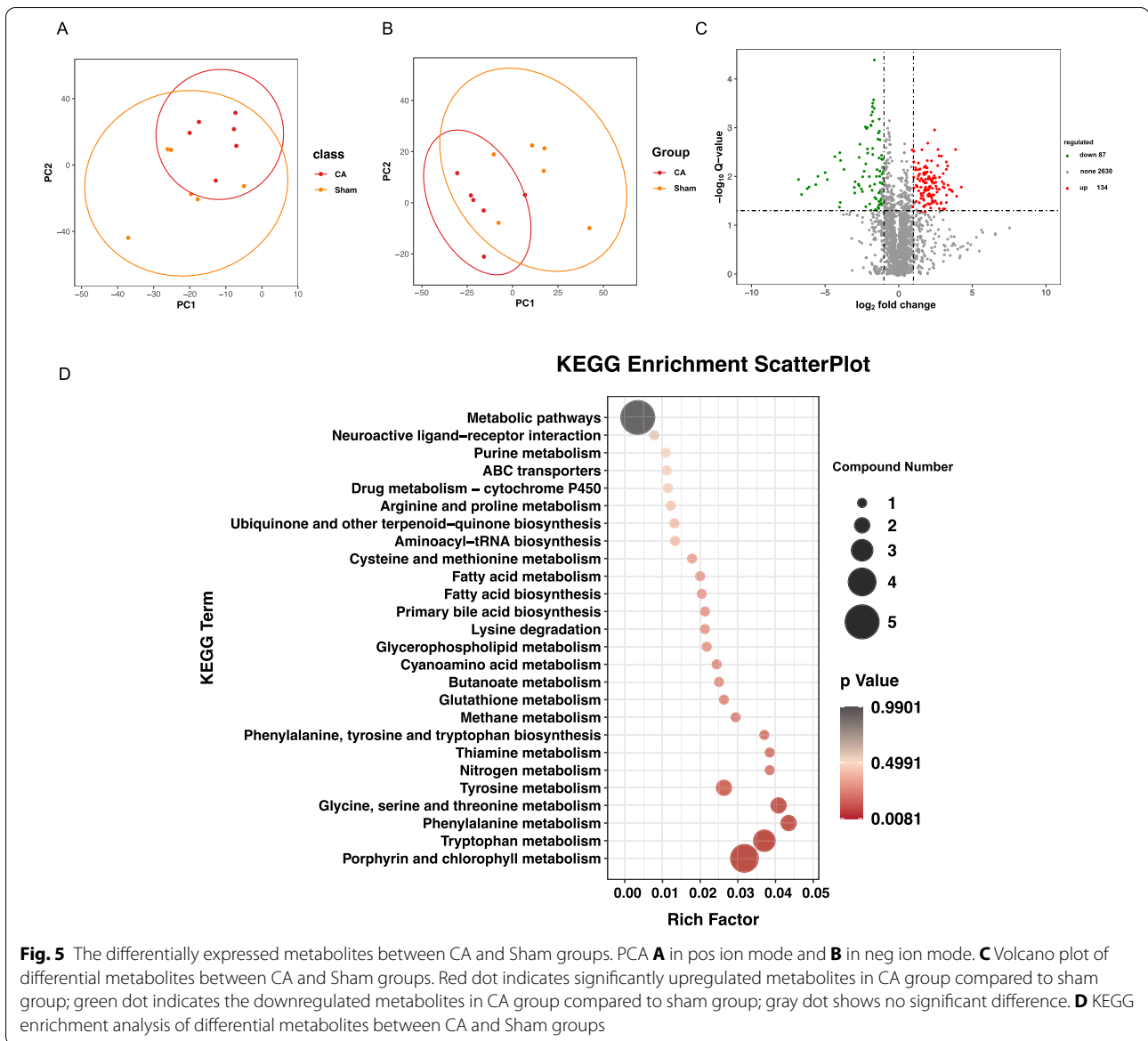
At the phylum level (Fig. 6A), *Verrucomicrobia* was positively correlated with palmitoleic acid, hexadecanedioic acid, acetyl-L-carnitine (ALC), palmitoylcarnitine, and glycine, while negatively correlated with indole, LPC (20:5). Similarly, *Actinobacteria* was positively correlated with indole, 3-indoleacetic acid, and LPC (20:5), while negatively correlated with palmitoleic acid. *Planctomycetes* were positively correlated with 3-indoleacetic acid, and negatively correlated with palmitoleic acid, palmitoylcarnitine, and glycine.

At the genus level (Fig. 6B), *Akkermansia* was positively correlated with glycine and ALC while negatively correlated with indole, 3-indoleacetic acid, and LPC (20:5), whereas *Romboutsia* was positively correlated with indole, 3-indoleacetic acid, and LPC (20:5), while

negatively correlated with glycine and ALC. Moreover, *Bifidobacterium* was positively correlated with indole, 3-indoleacetic acid, and LPC (20:5) and negatively correlated with ALC, while *Muribaculaceae_unclassified* was positively correlated with ALC and negatively correlated with indole, 3-indoleacetic acid and LPC (20:5). *Escherichia-Shigella* was positively correlated with glycine and ALC while negatively correlated with indole, 3-indoleacetic acid, and LPC (20:5).

Transcriptomics Analysis of CA Swine

Plasma metabolites might have an effect on CNS [27, 28]. To explore the postresuscitation molecular mechanism of encephalopathy, we performed transcriptome analysis of hippocampal tissue in both groups since the hippocampus was reported to be more sensitive to postresuscitation ischemia–reperfusion injury [29]. Combined with the fold change (ratio ≥ 2 or ratio ≤ 0.5) and Q value (< 0.05), a total of 163 DEGs were identified, among



which 112 were upregulated and 51 were downregulated (Fig. 7A).

The GO and KEGG pathway enrichment analysis was performed on DEGs. The GO enrichment analysis showed that DEGs were mainly enriched in extracellular space, neutrophil chemotaxis, activation of cysteine endopeptidase activity involved in apoptosis, activation of MAPKKK activity, inflammatory response, response of tumor necrosis factor to cells, and so on (Supplementary Fig. 4). Similarly, KEGG enrichment results showed that DEGs were mainly enriched in NF- κ B, IL-17, apoptosis, Fc epsilon RI, PPAR, cytokine-cytokine receptor interaction, Toll-like receptor, C-type lectin receptor, MAPK, RIG-I-like receptor, chemokine, apoptosis-multispecies,

complement and coagulation cascade, and FOXO signaling pathways (Fig. 7B). Previous studies reported activated NF- κ B, MAPK, and Toll-like signaling pathways by calcium overload and free radical production after cerebral ischemia-reperfusion, which increased the release of proinflammatory cytokines, resulting in neurological injury [30–32].

The differential gene interaction was analyzed using STRING database, which displayed 10 core genes, including *TNF*, *NCF2*, *CD14*, *S100A8*, *CD44*, *TIMP1*, *CCL3L1*, *NCF4*, *CCL4*, *S100A9*, and *PLAU* (Fig. 8), among which the top 10 core genes were found upregulated after resuscitation. Similar conclusions have been reported before, i.e., in a CA animal model, the TNF α levels in the CNS

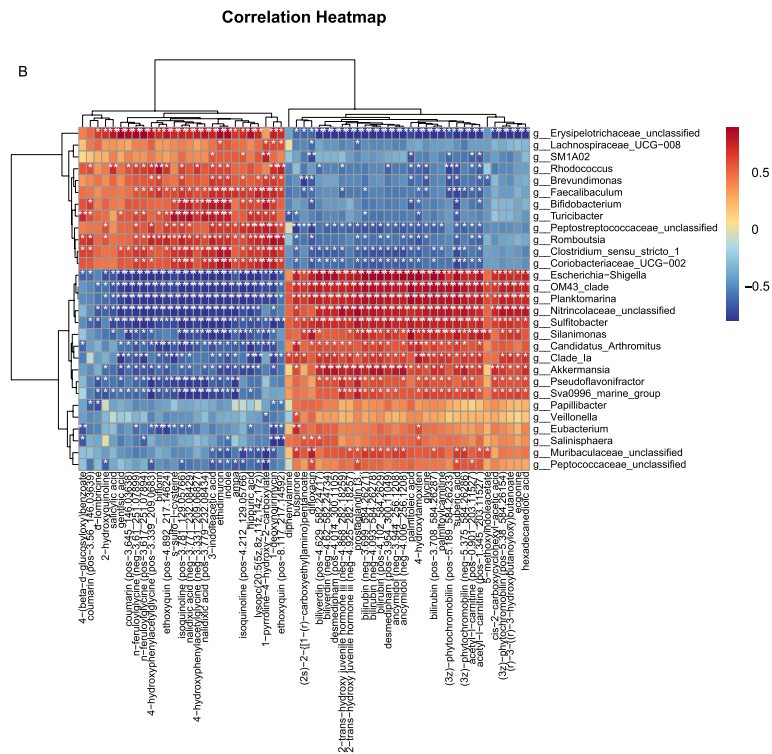
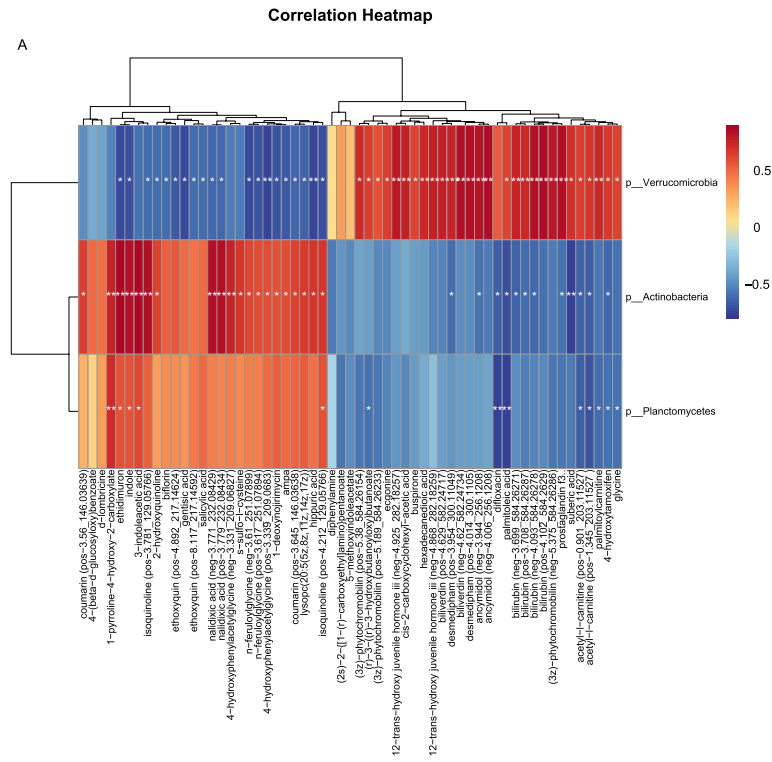
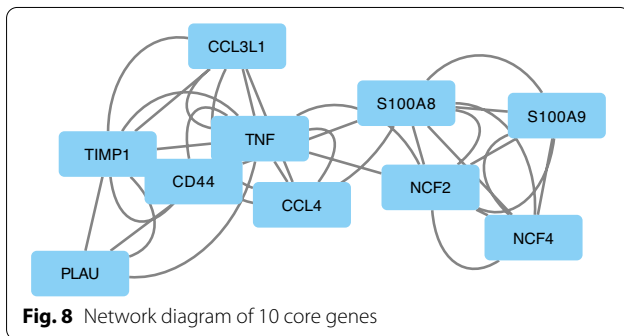
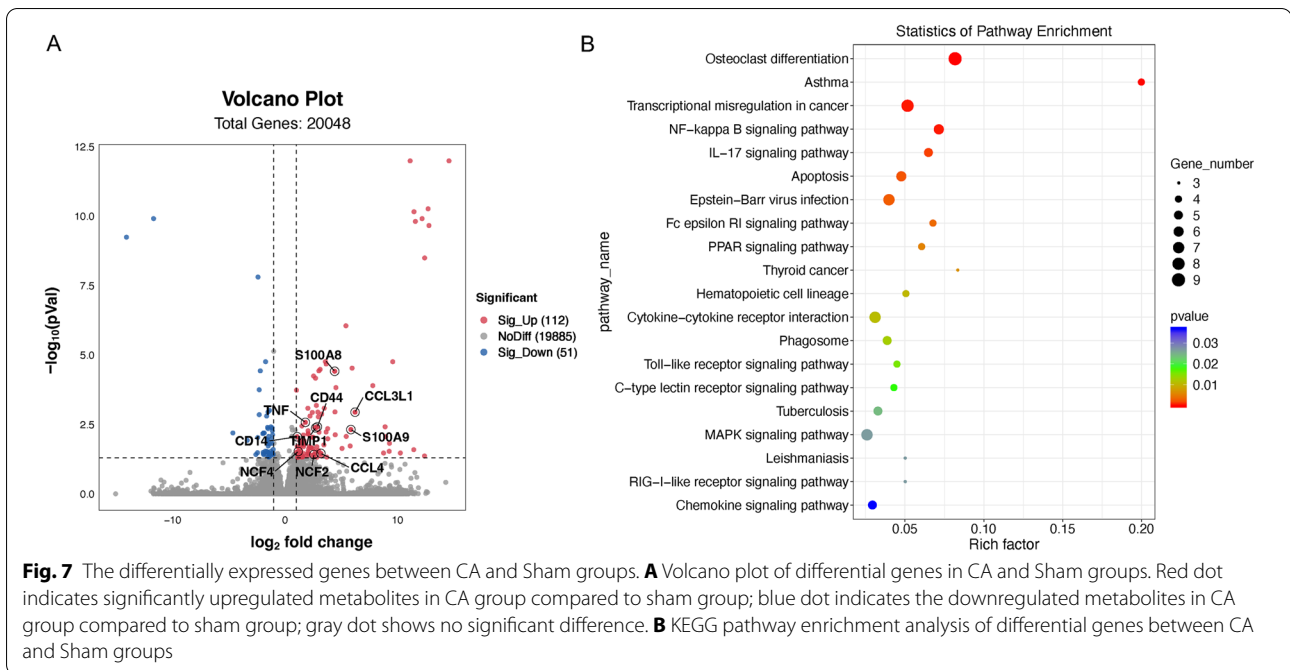


Fig. 6 Heatmap of correlation between the differential gut microbes and KEGG annotated differential metabolites. **A** Association between bacterial phyla and metabolites analyzed by spearman rank correlation analysis. **B** Association between bacterial genera and metabolites analyzed by spearman rank correlation analysis. Significant correlations ($P < 0.05$) are marked with "**." Positive correlations are indicated in red, and negative ones are shown in blue



were found to increase after resuscitation [33], while monocyte CD14 expression was found to gradually increase within 24 h after resuscitation and correlated with the duration from CA to ROSC [34]. In addition, upregulation of S100A8/9 expression was detected in brain tissue after cerebral ischemia–reperfusion injury [35, 36].

Correlations Between Metabolites and Genes

Several significant KEGG pathways were selected for further correlation analysis with metabolites (Supplementary Fig. 5). The resulting heat map showed that glycine was positively correlated with genes involved in apoptosis, IL-17, MAPK, NF-κB, and Toll-like receptor signaling pathways. Consistent with previous reports, glycine could modulate the expression of NF-κB to exert its anti-inflammatory effects [37].

Discussion

This study used a large animal model combined with multi-omics research to explore the changes in gut microbiota, plasma metabolites, and hippocampal transcriptional genes after resuscitation and their specific interactions. Gut microbiota data analysis showed that the CA group was rich in *Akkermansia* and *Muribaculaceae_unclassified* but insufficient in *Bifidobacterium* and *Romboutsia*, which might be potential biomarkers. The metabolomic study showed changes in amino acids and derivatives and lipid molecules after resuscitation, including significantly increased glycine and decreased D-lombricine after resuscitation. Moreover, transcriptomic analysis showed that the DEGs were mainly related to neuroinflammation and apoptosis. A relationship was observed between CA-related microbes and metabolites via integrated analysis of gut microbiota and metabolomics, where *Escherichia-Shigella* was positively correlated with glycine. Combined metabolomics and transcriptomics analysis showed that glycine was positively correlated with genes involved in apoptosis, IL-17, MAPK, NF-κB and Toll-like receptor signal pathways.

Establishment of VF-CA Swine Model

Animal models have been invaluable for exploring the etiology, pathogenesis, and intervention of CA. Swine are widely used as animal model CA research due to the anatomical and physiological similarities that swine share with humans [38]. The swine model in this study

simulated the clinical CA caused by VF. The methods of VF induction include electricity-induced VF and ischemia-induced VF. The electricity-induced VF is to place a fibrillation electrode in right ventricle through the jugular vein and apply electrical stimulation to the endocardium, triggering VF in a matter of seconds [26]. The ischemia-induced VF simulates the clinical situation of CA caused by myocardial ischemia. It is to occlude main collateral vessels of the coronary artery by interventional technique or thoracotomy, and VF is often induced within 5–10 min after severe ischemia [39]. Compared with ischemic-induced VF, the electricity-induced VF has the advantages of simple operation, less trauma, and can control the starting time of VF, which is repeatable and ensures the homogeneity of the animal model.

This study found that hemodynamics was unstable after resuscitation, which was characterized by decreased blood pressure, decreased cardiac output and increased heart rate, which was consistent with previous studies [26]. In addition, the significantly decreased NDS suggested the neurological injury after resuscitation, which proved the success on VF-CA swine model.

Gut Microbiota Dysbiosis After Resuscitation

The pathophysiologic mechanisms of neurological injury caused by CA and CPR are complicated. Several studies have found imbalanced gut microbiota and intestinal epithelial barrier injury after resuscitation, indicating that gut microbiota can regulate the pathogenesis of CA through the brain-gut axis. Using 16S rDNA gene sequencing, it was observed that there were significant differences in the richness and diversity of gut microbiota between the CA and sham groups. At the phylum level, compared with the sham group, the F/B ratio increased in the CA group, though *Firmicutes* and *Bacteroidetes* were still the dominant phylum in both groups. Studies have reported a changed F/B ratio as a sign of imbalanced gut microbiota [40, 41], suggesting gut microbiota dysbiosis after resuscitation in swine. Moreover, at the genus level, a total of 29 differential genera were identified, within increased *Muribaculaceae_unclassified*, *Akkermansia* and *Escherichia-Shigella* and decreased *Bifidobacterium* and *Romboutsia*. Of these, the four potential biomarkers in the CA group were *Akkermansia*, *Muribaculaceae_unclassified*, *Bifidobacterium* and *Romboutsia*.

In addition, the abundance of *A. muciniphila* increased after resuscitation, consistent with a previous study where *Akkermansia* and *A. muciniphila* were found to increase after stroke in rats [42]. *Akkermansia muciniphila*, an intestinal symbiont colonizing in the mucus layer, can specifically degrade mucin to produce short-chain fatty acids [43], which improves host metabolic functions and immune responses [44]. In

recent years, *A. muciniphila* was considered to be an important factor affecting human health, playing an important role in metabolic disorders, immune-related diseases and new treatments of cancer. However, some studies have reported the role of *A. muciniphila* in promoting inflammation. In the colitis mouse model induced by high glucose, it was observed that the abundance of *A. muciniphila* and the concentration of mucolytic enzymes increased, and the colonic mucus layer was eroded [45]. This is because *A. muciniphila* could secrete mucolytic enzymes such as glycosidase, which eroded the intestinal mucus layer, weakened the intestinal barrier function, made bacteria and endotoxin permeate, and aggravated inflammation. Therefore, it was inferred that increased *Akkermansia* may lead to impaired intestinal barrier and bacterial translocation after resuscitation, and inhibiting their proliferation may be a therapeutic target to improve outcomes in patients with CA.

Bifidobacterium are normal constituents of the gut microbial community and are known to promote intestinal health. *Bifidobacterium* supplementation could reduce the level of inflammatory factors in blood after stroke [46, 47], and promoted the long-term rehabilitation of stroke [48]. It can be inferred that *Bifidobacterium* has a protective effect on hypoxic-ischemic diseases. It has been reported that *Bifidobacterium* can reduce the production of plasma TMAO in mice by regulating the abundance of other intestinal microorganisms [49]. Nevertheless, the high level of TMAO was independently associated with hospital mortality and other adverse clinical outcomes in patients with OHCA [21]. In this study, the abundance of *Bifidobacterium* decreased after resuscitation, which might increase TMAO to promote inflammatory response, and exogenous supplement may be a therapeutic target to improve the prognosis of patients with CA.

Romboutsia can produce butyrate, which plays an important role in intestinal and immune regulation [50, 51]. Butyrate can increase intestinal probiotics [52], and repair ileal epithelial cells to improve intestinal permeability, reduce peripheral inflammatory response, reduce hippocampal nerve cell apoptosis, thus improve cognitive impairment after stroke [53]. In this study, the abundance of *Romboutsia* decreased after resuscitation, but no significant change of butyrate was observed in metabolites profiling. Similarly, *Muribaculaceae_unclassified*, as a probiotic, was related to butyric acid metabolism and tryptophan metabolism pathway [54], however, lacking studies regarding CA or ischemic-hypoxic encephalopathy. Whether *Romboutsia* and *Muribaculaceae_unclassified* can regulate nerve injury after resuscitation need to be further studied.

Escherichia coli is an opportunistic pathogenic bacterium [55]. Increased *Escherichia coli* can promote intestinal inflammation. In this study, the abundance of *Escherichia-Shigella* increased after resuscitation. Consistent with previous study, in the rat model of cerebral ischemia–reperfusion injury, it was also found that the abundance of *Escherichia coli* increased after hypoxic-ischemic [56]. In addition, when the abundance of *Escherichia coli* decreased after the specific intervention, the area of cerebral infarction decreased and the neurological function improved [57]. Inhibiting *Escherichia coli* proliferation may be a therapeutic target to improve outcomes in patients with CA.

Plasma Profile Changed After Resuscitation

Gut microbiota can regulate CNS through its metabolites; therefore, we explored the plasma metabolites in swine. Among the differential metabolites, we mainly focused on the changes of several amino acids and derivatives. Results showed that indole, 3-indoleacetic and D-lombicine were downregulated after resuscitation, while glycine was upregulated.

Tryptophan has three major metabolic routes: the kynurenine, serotonin, and the indolic pathway. In the present study, the levels of indole and its derivatives (indole-3-acetic acid) were found to decrease at 24 h after resuscitation, while serotonin derivatives (5-methoxyindole-3-acetic acid) increased, suggesting that tryptophan metabolism was changed after resuscitation. Although this study indicated the metabolic disorder of tryptophan, the results did not align with previous studies. In cerebral ischemia–reperfusion studies, tryptophan metabolism was reported to shift to the kynurenine pathway, i.e., primarily, the tryptophan level decreased in plasma, while the kynurenine level increased [20, 58, 59]. An increase in kynurenine levels was also observed in the hippocampus [20]. Studies have shown that the activation of the kynurenine pathway was associated with poor neurological outcomes after resuscitation [60], while kynurenine had a neuroprotective effect [61]. However, no kynurenine pathway activation was observed in the present study, which may be due to the metabolite's dynamic balance related to the time point observed after resuscitation. Giuseppe Ristagno et al. showed acutely altered tryptophan metabolism with decreased tryptophan and increased kynurenine within 2–4 h after resuscitation; however, tryptophan and kynurenine gradually recovered on the 3rd day after resuscitation [59].

Previous studies have reported the neuroprotective effect of glycine on cerebral ischemia–reperfusion injury [62], primarily by binding to the GluN2A (NMDA receptor subunit) to inhibit the neuroexcitotoxic effect of glutamate [63]. Similarly, glycine injection into the cerebral

ventricle of stroke rats showed that glycine inhibited M1 microglial polarization through the NF- κ B p65/Hif-1 α signal pathway [64]. In our results, the increased glycine level after resuscitation showed the compensatory neuroprotective effect of the body after the ischemia/hypoxia event. The enrichment of differential metabolic pathways suggested that glycine, serine and threonine metabolic pathways were significantly enriched, in which the identified differential metabolites were glycine and D-lombicine. From the KEGG map of glycine, serine and threonine, glycine and D-lombicine were found to be the downstream products of serine. The upregulated glycine and downregulated D-lombicine suggested the changed metabolic pattern of serine. We also found that glycine was associated with gut microbiota and was positively related to *Escherichia-Shigella*. *Escherichia coli* contains a gene *glyA* that encodes serine hydroxymethyltransferase (SHMT), which can promote the conversion of serine to glycine [65]. Previous studies have reported that Enterobacteriaceae proliferate through enhanced decomposition of L-serine in the inflamed gut [66]. *Escherichia-Shigella* might promoted the metabolism of serine to glycine.

Our results also showed that some lipids changed significantly after resuscitation, in which acylcarnitine and fatty acids were upregulated, and LPC was downregulated. Mitochondrial damage after resuscitation is one of the significant mechanisms of organ injury [17]. ALC promotes long-chain fatty acids from the cytoplasm to the mitochondria, where fatty acids β -oxidation occurs [67]. Therefore, ALC is vital in mitochondrial oxidative metabolism, protecting mitochondria from oxidative damage and inhibiting apoptosis caused by mitochondrial damage [68]. In cases of ischemia/hypoxia, incomplete oxidation of long-chain fatty acids accumulated in the cycle leads to the accumulation of acylcarnitine and fatty acids [69]. We identified 10 acylcarnitine and 4 fatty acids in the metabolomic profiling, all significantly upregulated after resuscitation, suggesting mitochondrial dysfunction after resuscitation. A clinical study showed that early application of ALC can improve the outcome of patients with stroke without reperfusion indication, since ALC can regulate neuroinflammation and oxidative stress after cerebral ischemia and play a neuroprotective role [70]. Another clinical study showed that higher ALC levels were associated with higher 30-day mortality and worse neurological outcomes in OHCA [71].

LPC is produced under the action of phospholipase A2 on phosphatidylcholine [72]. In vitro studies have shown that LPC protects against global cerebral ischemia and glutamate neuroexcitotoxic effects [73]. The in vivo and human results were consistent with the in vitro results. Mitsuaki Nishikimi et al. demonstrated that several LPCs

in human and rat plasma were significantly downregulated after resuscitation, and the decrease of plasma LPC level was correlated with poor survival outcome and neurological prognosis after resuscitation; additionally, LPC supplementation in the early resuscitation could improve the prognosis [74], which could be attributed to the anti-apoptotic and anti-inflammatory effects of LPC [75–77]. However, research on the relationship between LPC (20:5), found in this study, and CA is lacking.

Transcriptome Profile Changed After Resuscitation

Some metabolites could penetrate the brain to exert their effects through compromised blood–brain barrier. Thus, we analyzed after resuscitation changes in the hippocampal transcriptome. Our transcriptomic profiling identified 163 DEGs between the CA and sham group, among which the top 10 core genes (*TNF*, *NCF2*, *CD14*, *S100A8*, *CD44*, *TIMP1*, *CCL3L1*, *NCF4*, *CCL4*, and *S100A9*) were upregulated after resuscitation. Moreover, GO enrichment analysis suggested that inflammation response and apoptosis function were changed after resuscitation, while KEGG enrichment analysis indicated that differential genes were enriched in NF- κ B, Toll-like receptor, MAPK, Fc epsilon RI, and apoptosis signaling pathways, suggesting neuroinflammation and apoptosis occurred after resuscitation. In addition, we found that glycine was related to IL-17, apoptosis, NF- κ B, and MAPK signaling pathway genes, suggesting that glycine may play a neuroprotective role after resuscitation by influencing these pathways.

The *TNF* encodes a multifunctional proinflammatory cytokine, TNF- α , that belongs to the TNF superfamily and is a critical proinflammatory mediator in a range of acute brain injury [78], which can induce apoptosis, promote regeneration, and tissue repair [79], and its role is concentration dependent [79]. In the rat model of focal cerebral ischemia, the increased expression of *TNF* and TNF receptors was observed, alleviating the adverse effects of ischemia/reperfusion injury and having a neuroprotective effect [80]. TNF- α can activate the NF- κ B signal pathway through the TNF receptor [81], further inducing neural cells to produce proapoptotic genes and proteins, thereby initiating the caspase cascade reaction leading to cell apoptosis [82, 83]. The *NCF2* and *NCF4* are the activated components of the nicotinamide adenine dinucleotide phosphate oxidase complex, which will produce reactive oxygen species (ROS) once activated [84, 85]. The production of ROS was an important mechanism of brain injury after stroke, so the expression of the *NCF2* gene was increased after stroke [86]. Like brain injury after stroke, ischemia–reperfusion after resuscitation also leads to the production of ROS, accounting for the upregulated expression of *NCF2* and *NCF4* after

resuscitation in this study. Systemic ischemia–reperfusion injury after resuscitation leads to the increase of pathogen-associated molecular patterns, damage-associated molecular patterns, and the corresponding increase of pattern recognition receptors, such as Toll-like receptors. As a coreceptor of Toll-like receptor, CD14 has been shown to coordinate aseptic inflammatory response and cause cell damage [87], while *S100A8/9* has been proved to be a damage-associated molecular pattern family related to CNS injury playing a proinflammatory role through TLR4 [88]. Therefore, the neuroinflammation in HIBI after resuscitation might be related to the upregulated expression of *CD14* and *S100A8/9*.

This study has some strengths and limitations. The omics technology has the characteristics of high throughput, high sensitivity, and high accuracy. Bioinformatics can help us extract information from huge amounts of data. We represented the first attempt to analyze a multi-omics analysis of CA in a large animal model to explore the changes in gut microbiota, plasma metabolites, and hippocampal transcriptional genes after resuscitation and their specific interactions. The differential gut microbiota, metabolites, and genes were obtained via multi-omics analysis. This study is innovative and possesses a certain reference value. However, from the perspective of model establishment, we lacked the postresuscitation care, such as target temperature management, due to the limited experimental conditions. In addition, the role in HIBI after resuscitation remained unclear. Further verification experiments should be conducted in the future to refine our conclusions. In the later stage, the sample size had to be expanded for further in-depth research.

Conclusions

This study employed multi-omics analysis to explore the mechanism of HIBI after resuscitation. Generally, these altered gut microbiota and metabolites, and genes may be potential diagnosis biomarkers and therapeutic targets of HIBI, providing a theoretical foundation for future research on CA.

Supplementary Information

The online version contains supplementary material available at <https://doi.org/10.1007/s12028-024-02038-7>.

Abbreviations

ALC: Acetyl-L-carnitine; BBB: Blood-brain barrier; CA: Cardiac arrest; CNS: Central nervous system; CPR: Cardiopulmonary resuscitation; DAMP: Damage-associated molecular patterns; DEGs: Differentially expressed genes; FDR: False discovery rate; GEF: Global ejection function; HMDB: Human metabolome database; HIBI: Hypoxic-ischemic brain injury; HR: Heart rate; IL-17: Interleukin-17; KEGG: Kyoto encyclopedia of genes and genomes; MAP: Mean arterial pressure; NDSs: Neurological deficit scores; OHCA: Out-hospital cardiac arrest; PAMP: Pathogen-associated molecular patterns; PCA: Principal component analysis; PiCCO: Pulse index continuous cardiac output; PRRs: Pattern recognition receptors; ROS: Reactive oxygen species; ROSC: Return of spontaneous

circulation; SHMT: Serine hydroxymethyltransferase; SV: Stroke volume; TCA: Tricarboxylic acid cycle; TMAO: Trimethylamine-N-oxide; VF: Ventricular fibrillation; VIP: Variable important in projection.

Author details

¹ Department of Critical Care Medicine, Hangzhou First People's Hospital, Zhejiang University School of Medicine, Hangzhou, China. ² Department of Emergency Medicine, Second Affiliated Hospital, Zhejiang University School of Medicine, Hangzhou, China.

Acknowledgments

We thank all Department of Critical Care Medicine of Hangzhou First People's Hospital members for their helpful suggestions about the article.

Author Contributions

Shuhang Yu: Methodology, writing—original draft preparation. Jiefeng Xu: Investigation, formal analysis. Chenghao Wu: Investigation. Ying Zhu: Project administration. Mengyuan Diao: Writing—reviewing and editing. Wei Hu: Supervision, writing—reviewing and editing. The final manuscript was approved by all authors.

Source of Support

This work was supported by the National Natural Science Foundation of China (No. 82002008), Zhejiang Provincial Natural Science Foundation of China (No. LQ21H150001), and the Zhejiang Provincial Public Welfare Research Project (No. LGD20H150002), the Construction Fund of Medical Key Disciplines of Hangzhou (No. 0020200485), the Medical and Health Technology Project of Hangzhou (No. OO20190212), the Medical and Health Technology Project of Hangzhou (No. Z20220026).

Conflicts of interest

The authors declare that the research was conducted without any commercial or financial relationships that could be construed as a potential conflicts of interest.

Human and Animal Rights

The experimental protocol and procedures were approved by the Institutional Animal Care and Use Committee of the Second Affiliated Hospital, Zhejiang University School of Medicine. The experiment followed the Guide for the Care and Use of Laboratory Animals prepared by the Institute of Laboratory Animal Resources, published by the National Institutes of Health. The work was reported according to ARRIVE guideline.

Publisher's Note

Springer Nature remains neutral with regard to jurisdictional claims in published maps and institutional affiliations.

Springer Nature or its licensor (e.g. a society or other partner) holds exclusive rights to this article under a publishing agreement with the author(s) or other rightsholder(s); author self-archiving of the accepted manuscript version of this article is solely governed by the terms of such publishing agreement and applicable law.

Received: 31 January 2024 Accepted: 5 June 2024

Published online: 27 June 2024

References

- Holmberg MJ, Ross CE, Fitzmaurice GM, et al. Annual incidence of adult and pediatric in-hospital cardiac arrest in the United States. *Circ Cardiovasc Qual Outcomes*. 2019;12(7): e005580.
- Go AS, Mozaffarian D, Roger VL, et al. Heart disease and stroke statistics—2014 update: a report from the American Heart Association. *Circulation*. 2014;129(3):e28–292. <https://doi.org/10.1161/01.cir.0000441139.02102.80>.

- Wu L, Narasimhan B, Bhatia K, et al. Temporal trends in characteristics and outcomes associated with in-hospital cardiac arrest: a 20-year analysis (1999–2018). *J Am Heart Assoc*. 2021;10(23): e021572. <https://doi.org/10.1161/JAHA.121.021572>.
- Neumar RW, Nolan JP, Adrie C, et al. Post-cardiac arrest syndrome: epidemiology, pathophysiology, treatment, and prognostication. A consensus statement from the International Liaison Committee on Resuscitation (American Heart Association, Australian and New Zealand Council on Resuscitation, European Resuscitation Council, Heart and Stroke Foundation of Canada, InterAmerican Heart Foundation, Resuscitation Council of Asia, and the Resuscitation Council of Southern Africa); the American Heart Association Emergency Cardiovascular Care Committee; the Council on Cardiovascular Surgery and Anesthesia; the Council on Cardiopulmonary, Perioperative, and Critical Care; the Council on Clinical Cardiology; and the Stroke Council. *Circulation*. 2008;118(23):2452–83. <https://doi.org/10.1161/CIRCULATIONAHA.108.190652>.
- Sekhon MS, Ainslie PN, Griesdale DE. Clinical pathophysiology of hypoxic ischemic brain injury after cardiac arrest: a “two-hit” model. *Crit Care*. 2017;21(1):90. <https://doi.org/10.1186/s13054-017-1670-9>.
- Nolan JP, Neumar RW, Adrie C, et al. Post-cardiac arrest syndrome: epidemiology, pathophysiology, treatment, and prognostication. A Scientific Statement from the International Liaison Committee on Resuscitation; the American Heart Association Emergency Cardiovascular Care Committee; the Council on Cardiovascular Surgery and Anesthesia; the Council on Cardiopulmonary, Perioperative, and Critical Care; the Council on Clinical Cardiology; the Council on Stroke. *Resuscitation*. 2008;79(3):350–79. <https://doi.org/10.1016/j.resuscitation.2008.09.017>.
- Kim KS, Jeon MT, Kim ES, Lee CH, Kim DG. Activation of NMDA receptors in brain endothelial cells increases transcellular permeability. *Fluids Barriers CNS*. 2022;19(1):70. <https://doi.org/10.1186/s12987-022-00364-6>.
- Wagner SR, Lanier WL. Metabolism of glucose, glycogen, and high-energy phosphates during complete cerebral ischemia. A comparison of normoglycemic, chronically hyperglycemic diabetic, and acutely hyperglycemic nondiabetic rats. *Anesthesiology*. 1994;81(6):1516–26. <https://doi.org/10.1097/0000542-199412000-00028>.
- Sandrioni C, Cronberg T, Sekhon M. Brain injury after cardiac arrest: pathophysiology, treatment, and prognosis. *Intensive Care Med*. 2021;47(12):1393–414. <https://doi.org/10.1007/s00134-021-06548-2>.
- Yuan X, Chen B, Duan Z, et al. Depression and anxiety in patients with active ulcerative colitis: crosstalk of gut microbiota, metabolomics and proteomics. *Gut Microbes*. 2021;13(1):1987779. <https://doi.org/10.1080/19490976.2021.1987779>.
- Wu W, Sun Y, Luo N, et al. Integrated 16S rRNA gene sequencing and LC–MS analysis revealed the interplay between gut microbiota and plasma metabolites in rats with ischemic stroke. *J Mol Neurosci*. 2021;71(10):2095–106. <https://doi.org/10.1007/s12031-021-01828-4>.
- Gareau MG. The microbiota-gut-brain axis in sepsis-associated encephalopathy. *mSystems*. 2022;7(4): e0053322. <https://doi.org/10.1128/msystems.00533-22>.
- Sampson TR, Mazmanian SK. Control of brain development, function, and behavior by the microbiome. *Cell Host Microbe*. 2015;17(5):565–76. <https://doi.org/10.1016/j.chom.2015.04.011>.
- Zeng X, Li J, Shan W, Lai Z, Zuo Z. Gut microbiota of old mice worsens neurological outcome after brain ischemia via increased valeric acid and IL-17 in the blood. *Microbiome*. 2023;11(1):204. <https://doi.org/10.1186/s40168-023-01648-1>.
- Houlden A, Goldrick M, Brough D, et al. Brain injury induces specific changes in the caecal microbiota of mice via altered autonomic activity and mucoprotein production. *Brain Behav Immun*. 2016;57:10–20. <https://doi.org/10.1016/j.bbi.2016.04.003>.
- Choi J, Shoaib M, Yin T, et al. Tissue-specific metabolic profiles after prolonged cardiac arrest reveal brain metabolome dysfunction predominantly after resuscitation. *J Am Heart Assoc*. 2019;8(17): e012809. <https://doi.org/10.1161/JAHA.119.012809>.
- Shoaib M, Choudhary RC, Choi J, et al. Plasma metabolomics supports the use of long-duration cardiac arrest rodent model to study human disease by demonstrating similar metabolic alterations. *Sci Rep*. 2020;10(1):19707. <https://doi.org/10.1038/s41598-020-76401-x>.
- Paulin Beske R, Henriksen HH, Obling L, et al. Targeted plasma metabolomics in resuscitated comatose out-of-hospital cardiac arrest patients.

- Resuscitation. 2022;179:163–71. <https://doi.org/10.1016/j.resuscitation.2022.06.010>.
19. Agus A, Planchais J, Sokol H. Gut microbiota regulation of tryptophan metabolism in health and disease. *Cell Host Microbe*. 2018;23(6):716–24. <https://doi.org/10.1016/j.chom.2018.05.003>.
 20. Lucchetti J, Fumagalli F, Olivari D, et al. Brain kynurenine pathway and functional outcome of rats resuscitated from cardiac arrest. *J Am Heart Assoc*. 2021;10(23): e021071. <https://doi.org/10.1161/JAHA.121.021071>.
 21. Hochstrasser SR, Metzger K, Vincent AM, et al. Trimethylamine-N-oxide (TMAO) predicts short- and long-term mortality and poor neurological outcome in out-of-hospital cardiac arrest patients. *Clin Chem Lab Med*. 2020;59(2):393–402. <https://doi.org/10.1515/cclm-2020-0159>.
 22. Tissier R, Hocini H, Tchitchek N, et al. Early blood transcriptomic signature predicts patients' outcome after out-of-hospital cardiac arrest. *Resuscitation*. 2019;138:222–32. <https://doi.org/10.1016/j.resuscitation.2019.03.006>.
 23. Eun JW, Yang HD, Kim SH, et al. Identification of novel biomarkers for prediction of neurological prognosis following cardiac arrest. *Oncotarget*. 2017;8(10):16144–57. <https://doi.org/10.18632/oncotarget.14877>.
 24. Wang C, Qi C, Liu M, et al. Protective effects of agrimonolide on hypoxia-induced H9c2 cell injury by maintaining mitochondrial homeostasis. *J Cell Biochem*. 2022;123(2):306–21. <https://doi.org/10.1002/jcb.30169>.
 25. Wu H, Xu S, Diao M, Wang J, Zhang G, Xu J. Alda-1 treatment alleviates lung injury after cardiac arrest and resuscitation in swine. *Shock*. 2022;58(5):464–9. <https://doi.org/10.1097/SHK.0000000000002003>.
 26. Diao M, Xu J, Wang J, et al. Alda-1, an activator of ALDH2, improves postresuscitation cardiac and neurological outcomes by inhibiting pyroptosis in swine. *Neurochem Res*. 2022;47(4):1097–109. <https://doi.org/10.1007/s11064-021-03511-x>.
 27. Tu R, Xia J. Stroke and vascular cognitive impairment: the role of intestinal microbiota metabolite TMAO. *CNS Neurol Disord Drug Targets*. 2024;23(1):102–21. <https://doi.org/10.2174/1871527322666230203140805>.
 28. Ju S, Shin Y, Han S, et al. The gut-brain axis in schizophrenia: the implications of the gut microbiome and SCFA production. *Nutrients*. 2023;15(20):4391. <https://doi.org/10.3390/nu15204391>.
 29. Haglund M, Lindberg E, Englund E. Hippocampus and basal ganglia as potential sentinel sites for ischemic pathology after resuscitated cardiac arrest. *Resuscitation*. 2019;139:230–3. <https://doi.org/10.1016/j.resuscitation.2019.04.012>.
 30. Zhao H, Li CS, Gong P, et al. Molecular mechanisms of therapeutic hypothermia on neurological function in a swine model of cardiopulmonary resuscitation. *Resuscitation*. 2012;83(7):913–20. <https://doi.org/10.1016/j.resuscitation.2012.01.001>.
 31. Barone FC, Irving EA, Ray AM, et al. Inhibition of p38 mitogen-activated protein kinase provides neuroprotection in cerebral focal ischemia. *Med Res Rev*. 2001;21(2):129–45. [https://doi.org/10.1002/1098-1128\(200103\)21:2%3c129::aid-med1003%3e3.0.co;2-h](https://doi.org/10.1002/1098-1128(200103)21:2%3c129::aid-med1003%3e3.0.co;2-h).
 32. Asmussen A, Fink K, Busch HJ, et al. Inflammasome and toll-like receptor signaling in human monocytes after successful cardiopulmonary resuscitation. *Crit Care*. 2016;20(1):170. <https://doi.org/10.1186/s13054-016-1340-3>.
 33. Janata A, Magnet IA, Uray T, et al. Regional TNFalpha mapping in the brain reveals the striatum as a neuroinflammatory target after ventricular fibrillation cardiac arrest in rats. *Resuscitation*. 2014;85(5):694–701. <https://doi.org/10.1016/j.resuscitation.2014.01.033>.
 34. Asmussen A, Busch HJ, Helbing T, et al. Monocyte subset distribution and surface expression of HLA-DR and CD14 in patients after cardiopulmonary resuscitation. *Sci Rep*. 2021;11(1):12403. <https://doi.org/10.1038/s41598-021-91948-z>.
 35. Sun P, Li Q, Zhang Q, Xu L, Han JY. Upregulated expression of S100A8 in mice brain after focal cerebral ischemia reperfusion. *World J Emerg Med*. 2013;4(3):210–4. <https://doi.org/10.5847/wjem.j.issn.1920-8642.2013.03.010>.
 36. Shichita T, Ito M, Morita R, et al. MAFB prevents excess inflammation after ischemic stroke by accelerating clearance of damage signals through MSR1. *Nat Med*. 2017;23(6):723–32. <https://doi.org/10.1038/nm.4312>.
 37. Aguayo-Ceron KA, Sanchez-Munoz F, Gutierrez-Rojas RA, et al. Glycine: the smallest anti-inflammatory micronutrient. *Int J Mol Sci*. 2023;24(14):11236. <https://doi.org/10.3390/ijms241411236>.
 38. Baroux D, Chalkias A, Syggelou A, Iacovidou N, Xanthos T. Research in human resuscitation: what we learn from animals. *J Matern Fetal Neonatal Med*. 2012;25(Suppl 5):44–6. <https://doi.org/10.3109/14767058.2012.714633>.
 39. Indik JH, Allen D, Shanmugasundaram M, et al. Predictors of resuscitation in a swine model of ischemic and nonischemic ventricular fibrillation cardiac arrest: superiority of amplitude spectral area and slope to predict a return of spontaneous circulation when resuscitation efforts are prolonged. *Crit Care Med*. 2010;38(12):2352–7. <https://doi.org/10.1097/CCM.0b013e3181fa01ee>.
 40. Lucas C, Barnich N, Nguyen HT. Microbiota, inflammation and colorectal cancer. *Int J Mol Sci*. 2017;18(6):1310. <https://doi.org/10.3390/ijms18061310>.
 41. Grigor'eva IN. Gallstone disease, obesity and the Firmicutes/Bacteroidetes ratio as a possible biomarker of gut dysbiosis. *J Pers Med*. 2020;11(1):13. <https://doi.org/10.3390/jpm11010013>.
 42. Lin H, Chen S, Shen L, et al. Integrated analysis of the cecal microbiome and plasma metabolomics to explore NaoMaiTong and its potential role in changing the intestinal flora and their metabolites in ischemic stroke. *Front Pharmacol*. 2021;12:773722. <https://doi.org/10.3389/fphar.2021.773722>.
 43. Liu MJ, Yang JY, Yan ZH, et al. Recent findings in Akkermansia muciniphila-regulated metabolism and its role in intestinal diseases. *Clin Nutr*. 2022;41(10):2333–44. <https://doi.org/10.1016/j.clnu.2022.08.029>.
 44. Zhang T, Li Q, Cheng L, Buch H, Zhang F. Akkermansia muciniphila is a promising probiotic. *Microb Biotechnol*. 2019;12(6):1109–25. <https://doi.org/10.1111/1751-7915.13410>.
 45. Khan S, Waliullah S, Godfrey V, et al. Dietary simple sugars alter microbial ecology in the gut and promote colitis in mice. *Sci Transl Med*. 2020;12(567):eaay6218. <https://doi.org/10.1126/scitranslmed.aay6218>.
 46. Wang Y, Zhang X, Wang Y, et al. Effects of combined live bifidobacterium, lactobacillus, enterococcus and bacillus cereus tablets on post-stroke depression and serum inflammatory factors. *Discov Med*. 2023;35(176):312–20. <https://doi.org/10.24976/Discov.Med.202335176.32>.
 47. Kang Y, Yang Y, Wang J, Ma Y, Cheng H, Wan D. Correlation between intestinal flora and serum inflammatory factors in post-stroke depression in ischemic stroke. *J Coll Physicians Surg Pak*. 2021;31(10):1224–7. <https://doi.org/10.29271/jcpsp.2021.10.1224>.
 48. Huang JT, Mao YQ, Han B, et al. Calorie restriction conferred improvement effect on long-term rehabilitation of ischemic stroke via gut microbiota. *Pharmacol Res*. 2021;170:105726. <https://doi.org/10.1016/j.phrs.2021.105726>.
 49. Wang Q, Guo M, Liu Y, et al. *Bifidobacterium breve* and *Bifidobacterium longum* attenuate choline-induced plasma trimethylamine N-oxide production by modulating gut microbiota in mice. *Nutrients*. 2022;14(6):1222. <https://doi.org/10.3390/nu14061222>.
 50. Hu YH, Meyer K, Lulla A, et al. Gut microbiome and stages of diabetes in middle-aged adults: CARDIA microbiome study. *Nutr Metab (Lond)*. 2023;20(1):3. <https://doi.org/10.1186/s12986-022-00721-0>.
 51. Chen Z, Radjabzadeh D, Chen L, et al. Association of insulin resistance and type 2 diabetes with gut microbial diversity: a microbiome-wide analysis from population studies. *JAMA Netw Open*. 2021;4(7):e2118811. <https://doi.org/10.1001/jamanetworkopen.2021.18811>.
 52. Chen R, Xu Y, Wu P, et al. Transplantation of fecal microbiota rich in short chain fatty acids and butyric acid treat cerebral ischemic stroke by regulating gut microbiota. *Pharmacol Res*. 2019;148:104403. <https://doi.org/10.1016/j.phrs.2019.104403>.
 53. Wang H, Zhang M, Li J, et al. Gut microbiota is causally associated with poststroke cognitive impairment through lipopolysaccharide and butyrate. *J Neuroinflamm*. 2022;19(1):76. <https://doi.org/10.1186/s12974-022-02435-9>.
 54. Wang J, Han L, Liu Z, et al. Genus unclassified_Muribaculaceae and microbiota-derived butyrate and indole-3-propionic acid are involved in benzene-induced hematopoietic injury in mice. *Chemosphere*. 2023;313:137499. <https://doi.org/10.1016/j.chemosphere.2022.137499>.
 55. Del Prete S, Bua S, Supuran CT, Capasso C. Escherichia coli gamma-carboxylic anhydrase: characterisation and effects of simple aromatic/heterocyclic sulphonamide inhibitors. *J Enzyme Inhib Med Chem*. 2020;35(1):1545–54. <https://doi.org/10.1080/14756366.2020.1800670>.
 56. Ding X, Liu Z, Liu Y, et al. Comprehensive evaluation of the mechanism of *Gastrodia elata* Blume in ameliorating cerebral ischemia-reperfusion injury based on integrating fecal metabolomics and 16S rDNA

- sequencing. *Front Cell Infect Microbiol.* 2022;12:1026627. <https://doi.org/10.3389/fcimb.2022.1026627>.
57. Xian M, Shen L, Zhan S, et al. Integrated 16S rRNA gene sequencing and LC/MS-based metabolomics ascertained synergistic influences of the combination of acupuncture and NaoMaiTong on ischemic stroke. *J Ethnopharmacol.* 2022;293: 115281. <https://doi.org/10.1016/j.jep.2022.115281>.
58. Ristagno G, Latini R, Vaahersalo J, et al. Early activation of the kynurenine pathway predicts early death and long-term outcome in patients resuscitated from out-of-hospital cardiac arrest. *J Am Heart Assoc.* 2014;3(4): e001094. <https://doi.org/10.1161/JAHA.114.001094>.
59. Ristagno G, Fries M, Brunelli L, et al. Early kynurenine pathway activation following cardiac arrest in rats, pigs, and humans. *Resuscitation.* 2013;84(11):1604–10. <https://doi.org/10.1016/j.resuscitation.2013.06.002>.
60. Loretz N, Becker C, Hochstrasser S, et al. Activation of the kynurenine pathway predicts mortality and neurological outcome in cardiac arrest patients: a validation study. *J Crit Care.* 2022;67:57–65. <https://doi.org/10.1016/j.jcrc.2021.09.025>.
61. Stone TW. Development and therapeutic potential of kynurenic acid and kynurenine derivatives for neuroprotection. *Trends Pharmacol Sci.* 2000;21(4):149–54. [https://doi.org/10.1016/s0165-6147\(00\)01451-6](https://doi.org/10.1016/s0165-6147(00)01451-6).
62. Tanabe M, Nitta A, Ono H. Neuroprotection via strychnine-sensitive glycine receptors during post-ischemic recovery of excitatory synaptic transmission in the hippocampus. *J Pharmacol Sci.* 2010;113(4):378–86. <https://doi.org/10.1254/jphs.10150fp>.
63. Hu R, Chen J, Lujan B, et al. Glycine triggers a non-ionotropic activity of GluN2A-containing NMDA receptors to confer neuroprotection. *Sci Rep.* 2016;6:34459. <https://doi.org/10.1038/srep34459>.
64. Liu R, Liao XY, Pan MX, et al. Glycine exhibits neuroprotective effects in ischemic stroke in rats through the inhibition of M1 microglial polarization via the NF-kappaB p65/Hif-1alpha signaling pathway. *J Immunol.* 2019;202(6):1704–14. <https://doi.org/10.4049/jimmunol.1801166>.
65. Teng Z, Pan X, Liu Y, et al. Engineering serine hydroxymethyltransferases for efficient synthesis of L-serine in *Escherichia coli*. *Bioresour Technol.* 2023;393: 130153. <https://doi.org/10.1016/j.biortech.2023.130153>.
66. Kitamoto S, Alteri CJ, Rodrigues M, et al. Dietary L-serine confers a competitive fitness advantage to Enterobacteriaceae in the inflamed gut. *Nat Microbiol.* 2020;5(1):116–25. <https://doi.org/10.1038/s41564-019-0591-6>.
67. Traina G. The neurobiology of acetyl-L-carnitine. *Front Biosci (Landmark Ed).* 2016;21(7):1314–29. <https://doi.org/10.2741/4459>.
68. Pourshahidi S, Shamsiri AR, Derakhshan S, Mohammadi S, Ghorbani M. The effect of acetyl-L-carnitine (ALCAR) on peripheral nerve regeneration in animal models: a systematic review. *Neurochem Res.* 2023;48(8):2335–44. <https://doi.org/10.1007/s11064-023-03911-1>.
69. Fillmore N, Mori J, Lopaschuk GD. Mitochondrial fatty acid oxidation alterations in heart failure, ischaemic heart disease and diabetic cardiomyopathy. *Br J Pharmacol.* 2014;171(8):2080–90. <https://doi.org/10.1111/bph.12475>.
70. Mazdeh M, Abolfathi P, Sabetghadam M, Mohammadi Y, Mehrpooya M. Clinical evidence of acetyl-L-carnitine efficacy in the treatment of acute ischemic stroke: a pilot clinical trial. *Oxid Med Cell Longev.* 2022;2022:2493053. <https://doi.org/10.1155/2022/2493053>.
71. Widmer M, Thommen EB, Becker C, et al. Association of acyl carnitines and mortality in out-of-hospital-cardiac-arrest patients: results of a prospective observational study. *J Crit Care.* 2020;58:20–6. <https://doi.org/10.1016/j.jcrc.2020.03.009>.
72. Dorninger F, Moser AB, Kou J, et al. Alterations in the plasma levels of specific choline phospholipids in Alzheimer's disease mimic accelerated aging. *J Alzheimers Dis.* 2018;62(2):841–54. <https://doi.org/10.3233/JAD-171036>.
73. Blondeau N, Lauritzen I, Widmann C, Lazdunski M, Heurteaux C. A potent protective role of lysophospholipids against global cerebral ischemia and glutamate excitotoxicity in neuronal cultures. *J Cereb Blood Flow Metab.* 2002;22(7):821–34. <https://doi.org/10.1097/00004647-200207000-00007>.
74. Nishikimi M, Yagi T, Shoaib M, et al. Phospholipid screening postcardiac arrest detects decreased plasma lysophosphatidylcholine: supplementation as a new therapeutic approach. *Crit Care Med.* 2022;50(2):e199–208. <https://doi.org/10.1097/CCM.00000000000005180>.
75. Ikeno Y, Cheon SH, Konno N, Nakamura A, Kitamoto K, Arioka M. Lysophosphatidylcholine protects cerebellar granule neurons from apoptotic cell death. *J Neurosci Res.* 2009;87(1):190–9. <https://doi.org/10.1002/jnr.21821>.
76. Minamihata T, Takano K, Moriyama M, Nakamura Y. Lysophosphatidylinositol, an endogenous ligand for G protein-coupled receptor 55, has anti-inflammatory effects in cultured microglia. *Inflammation.* 2020;43(5):1971–87. <https://doi.org/10.1007/s10753-020-01271-4>.
77. Knuplez E, Marsche G. An updated review of pro- and anti-inflammatory properties of plasma lysophosphatidylcholines in the vascular system. *Int J Mol Sci.* 2020;21(12):4501. <https://doi.org/10.3390/ijms21124501>.
78. Nawashiro H, Martin D, Hallenbeck JM. Neuroprotective effects of TNF binding protein in focal cerebral ischemia. *Brain Res.* 1997;778(2):265–71. [https://doi.org/10.1016/s0006-8993\(97\)00981-5](https://doi.org/10.1016/s0006-8993(97)00981-5).
79. Barnum CJ, Tansey MG. The duality of TNF signaling outcomes in the brain: Potential mechanisms? *Exp Neurol.* 2011;229(2):198–200. <https://doi.org/10.1016/j.expneurol.2011.02.016>.
80. Dornbos D 3rd, Ding Y. Mechanisms of neuronal damage and neuroprotection underlying ischemia/reperfusion injury after physical exercise. *Curr Drug Targets.* 2012;13(2):247–62. <https://doi.org/10.2174/138945012799201658>.
81. Hayden MS, West AP, Ghosh S. SnapShot: NF-kappaB signaling pathways. *Cell.* 2006;127(6):1286–7. <https://doi.org/10.1016/j.cell.2006.12.005>.
82. Zingarelli B, Hake PW, O'Connor M, Denenberg A, Kong S, Aronow BJ. Absence of poly(ADP-ribose)polymerase-1 alters nuclear factor-kappa B activation and gene expression of apoptosis regulators after reperfusion injury. *Mol Med.* 2003;9(5–8):143–53. <https://doi.org/10.2119/2003-00011.zingarelli>.
83. Niu YL, Zhang WJ, Wu P, et al. Expression of the apoptosis-related proteins caspase-3 and NF-kappaB in the hippocampus of Tg2576 mice. *Neurosci Bull.* 2010;26(1):37–46. <https://doi.org/10.1007/s12264-010-6122-3>.
84. Nauseef WM. Assembly of the phagocyte NADPH oxidase. *Histochem Cell Biol.* 2004;122(4):277–91. <https://doi.org/10.1007/s00418-004-0679-8>.
85. Anderson KE, Chessa TA, Davidson K, et al. PtdIns3P and Rac direct the assembly of the NADPH oxidase on a novel, pre-phagosomal compartment during FcR-mediated phagocytosis in primary mouse neutrophils. *Blood.* 2010;116(23):4978–89. <https://doi.org/10.1182/blood-2010-03-275602>.
86. Shibata K, Hashimoto T, Nobe K, Hasumi K, Honda K. Neuroprotective mechanisms of SMTP-7 in cerebral infarction model in mice. *Naunyn Schmiedeberg Arch Pharmacol.* 2011;384(1):103–8. <https://doi.org/10.1007/s00210-011-0642-x>.
87. Chen GY, Nunez G. Sterile inflammation: sensing and reacting to damage. *Nat Rev Immunol.* 2010;10(12):826–37. <https://doi.org/10.1038/nri2873>.
88. Vogl T, Tenbrock K, Ludwig S, et al. Mrp8 and Mrp14 are endogenous activators of Toll-like receptor 4, promoting lethal, endotoxin-induced shock. *Nat Med.* 2007;13(9):1042–9. <https://doi.org/10.1038/nm1638>.